JACS
JOURNAL OF THE AMERICAN CHEMICAL SOCIETY
Article
pubs.acs.org/JACS

Multiple Pathways for the Primary Step of the Spiropyran Photochromic Reaction: A CASPT2//CASSCF Study

Fengyi Liu and Keiji Morokuma*

Fukui Institute for Fundamental Chemistry, Kyoto University, Kyoto 606-8103, Japan

Supporting Information

ABSTRACT: CASSCF and CASPT2 studies on the reaction mechanism of the photochromic ring-opening process of a spiropyran (SP) (1′,3′,3′-trimethylspiro-[2*H*-1-benzopyran-2,2′-indoline], also known as BIPS) have been performed and possible excited-state C−O (and C−N) bond cleavage pathways and S_1-to-S_0 nonadiabatic transition channels have been explored. (1) The C−O bond dissociation in SP does not follow a conical-intersection mechanism that has been proposed in a model study with a simplified benzopyran. The CASSCF-optimized crossing points are actually avoided crossings with a large S_1-S_0 energy gap at the CASPT2 level; thus, they could not act as efficient S_1-to-S_0 funnels. (2) C−O bond cleavage paths on S_1 leading to both the CCC (cis−cis−cis with respect to the configuration around α, β, γ) and TCC (trans−cis−cis) intermediates of merocyanine (MC) are barrierless, in line with the experimentally observed ultrafast formation of MC. (3) An unexpected low-energy hydrogen-out-of-plane (HOOP) valley on the ($\pi\rightarrow\sigma^*$) surface was located not far from the C−O bond cleavage path and was suggested to be an efficient S_1-to-S_0 nonadiabatic decay channel. Triggered by the active HOOP mode, the molecule can easily access the S_1−HOOP valley and then make a transition to the S_0 surface through the narrow S_1-S_0 gap that exists in an extended region. Nonadiabatic decay through a conical intersection on C−N dissociation path as well as the HOOP funnel is responsible for high internal conversion yields of SP. These findings shedding light on the complex mechanism of SP−MC interconversion provide fundamental information for design spiropyran-based photochromic devices.

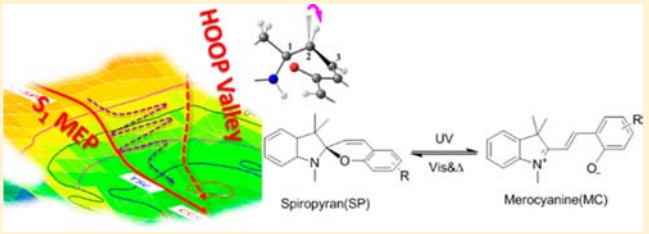

1. INTRODUCTION

Photochromic interconversion of spiropyran (SP) and merocyanine (MC) has been the subject of many recent studies in a wide range of fields, such as optical data storage,[1,2] optical switch,[3−9] optical nanoparticle,[10−12] and photonic crystal.[13,14] As shown in Chart 1, irradiation of ultraviolet

Chart 1

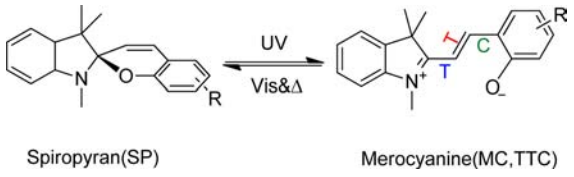

light converts SP into the open, colored MC form, while heating or irradiation in the visible region switches MC back to the colorless SP form. The reversible transformation, accompanied by remarkable changes in geometries and charge distribution, gives rise to distinctively different photopysical properties of the two forms and inspires many fascinating designs in various application fields.

Due to their importance in industrial applications, photochemical reactions of SP have been extensively studied by time-resolved spectroscopy.[15−22] Findings of these experiments shed light on the complex mechanism that accomplishes drastic changes in structures in one reaction. It is generally accepted that the initial step of the photoisomerization is the C−O bond cleavage between the spiro carbon (C1 in Chart 2) and oxygen,

Chart 2

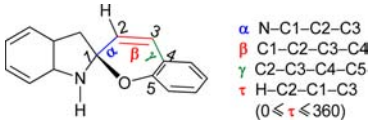

which typically takes place on a time scale from subpico- to picosecond. After this step, a cisoid open-form intermediate is probably formed, followed by geometrical rearrangements to planar MC forms on pico- to nanosecond scale, depending on the substituents on the chromene units (Chart 1) and experimental conditions. The most stable MC form in solution is trans−trans−cis (TTC, with respect to the configuration around α, β, γ in Chart 2). In addition to the dynamics, the mechanism also shows significant substituent dependence. For instance, the ring-opening reaction of unsubstituted SP (1′,3′,3′-trimethylspiro-[2*H*-1-benzopyran-2,2′-indoline], known as BIPS) involves only singlet states,[17] while for its

Received: March 21, 2013
Published: July 2, 2013

   dx.doi.org/10.1021/ja402868b | *J. Am. Chem. Soc.* 2013, 135, 10693−10702

NO_2-subtituted derivative (6-nitro-BIPS) a triplet state is found to play a role in the reaction.[16]

Considering the complexity of the reaction, in the current work we focus our attention on the primary step of the reaction, namely the ring-opening process, for unsubstituted BIPS (three methyl groups in 1′,3′,3′-positions replaced by hydrogen, as seen in Chart 2). Some aspects of the reaction have been revealed by spectroscopic investigations. A subpicosecond transient spectroscopic study by Ernsting and Arthen-Engeland suggested an ultrafast formation of MC form in 0.9 ps. On the basis of this, the authors proposed that the S_1-state reaction is likely to be barrierless.[17] However, their finding has been unsupported by a later femtosecond UV−mid-IR pump−probe study of Rini et al.[18] They reported a remarkably slower (28 ps) time constant for MC formation. The major decay channel for the S_1 excited state of the BIPS is suggested to be a very efficient (quantum yields 90%) and rapid internal conversion (IC) path to the SP ground state, leaving less than 10% for ring-opening reaction (to the MC form). Therefore, the efficient IC in SP is a major drawback to photochromic application. Although the experimental techniques did not allow for the authors to identify an intermediate species/state, they concluded that MC products are clearly not formed directly from the S_1 state of SP. Actually, the authors proposed that a large number of intermediates could be involved. Very recently, dynamics of a water-soluble derivative of SP (known as Py-BIPS) has been investigated by femtosecond absorption spectroscopy in aqueous solution.[22] The results of Kohl-Landgraf and coauthors confirmed a very efficient IC path as well as low quantum yields of MC products (3.3%), in good agreement with the findings of Rini et al. in the gas phase.[18] However, the measured MC formation time constant, 1.6 ps, is much faster. Except for these experimental findings, details of the ring-opening process are still ambiguous and need to be unraveled.

Compared to a substantial number of experimental reports, theoretical efforts aimed at the excited-state reaction mechanism of the SP ring-opening reaction are rather limited. The large size of SP has restricted calculations with suitable quantum chemical methodologies. Two theoretical studies treating only simplified models of SP have been published for excited states at the complete active space self-consistent field (CASSCF)[23] and complete active space second-order perturbation theory (CASPT2)[24] level.[25,26] A pioneering work by Robb's group used a benzopyran (chromene, which also exhibits photochromism) molecule as the model compound.[25] On the basis of their CASSCF and CASPT2//CASSCF calculations, a reaction mechanism via a conical intersection (CI)[27] has been proposed, which described well the reaction of the model compound. For the model compound, the reaction takes place along the (n→π^*) excited state, which is reached after the initial excitation and decays to the ground state of the product through a CI. As will be shown later, the photochemistry of SP is quite more complicated than that of this model system. Recently, another CASSCF(14e/12o) and CASPT2//CASSCF study with a more realistic model (denoted as *m*SP), in which the indoline subunit in SP (Chart 1) is simplified to a pyrroline, was reported by Sanchez-Lozano and co-workers.[26] Two possible ultrafast routes for efficient conversion to the ground state were suggested: one involves the rupture of the C_{spiro}−O bond leading to the open form and the other involves the lengthening of the C_{spiro}−N bond with no photoreaction. In addition, reaction paths to the different S_1/S_0 conical intersections were studied using interpolated reaction paths. It has been found previously by us (and by many others) that mimicking a photochemical process with a small model must be done with great caution.[28−30] This is especially crucial when conjugated moieties are truncated and/or the reaction mechanism is focused on, since the simplified model does not represent the conformational flexibility of the real molecule and sometimes may miss important excitation involving the π moieties.

To shed light on the mechanism of SP photochromic reaction, especially for the primary ring-opening step, we have carried out CASSCF and CASPT2//CASSCF calculations for an unsubstituted SP molecule (in which three methyl groups are replaced by hydrogen to save computation costs) to follow the minimal energy paths on S_1 surface along the C−O and C−N bond stretching coordinates. The results including all excited-state reaction paths as well as important nonadiabatic decay to ground states are presented in this paper to clarify the complex mechanism of real photochromic SP−MC interconversion.

2. COMPUTATIONAL DETAILS

The geometries of the ground state and two low-lying singlet excited states of SP were optimized at the CASSCF level of theory with the 6-31G(d) basis sets.[31] The state-averaged CASSCF (SA-CASSCF) method was used, allowing for a balanced description of the investigated states, especially at the closely interacting region. The three-state average (SA3) CASSCF wave function has been found to be capable of adequately describing all necessary states involved the photoinduced bond cleavage processes.

Our strategy for the CASSCF calculations is aimed at finding a proper active space that is capable of describing different stages of the reaction, i.e., the initial photoexcitation of SP and relaxation around the Franck−Condon (FC) geometry, the C−O (or C−N) bond cleavage, and the formation of an extended π system in MC. Therefore, a reasonable active space needs to include the bonding and antibonding σ and σ^* orbital of C−O bond, one pair of π and π^* orbitals on the indoline unit, and three π and two π^* orbitals on the chromene unit as well as the formed oxygen lone-pair orbital of MC. The finally constructed active space consists of 12 electrons distributed in 10 orbitals, therefore denoted as CAS(12e/10o). In the case of C−N bond cleavage, the bonding and antibonding σ and σ^* orbital of C−N bond, instead of that of C−O bond, are included in the active space. The corresponding active space is denoted as $CAS(12e/10o)_{CN}$. The nature of the active orbitals can be found in the Supporting Information (Figure S1).

In addition to the ground- and excited-state minima, the minimum energy paths (MEPs) on the S_0 and S_1 states are obtained at the same level of theory by using a similar strategy as described in our previous work.[32] Following the C_1−O (or C_1−N) stretching and the torsional α around the C_1−C_2 bond, quasi-2D potential energy surfaces (PESs) were constructed by a series of constrained geometry optimizations. The minimum energy conical intersection (MECI) between the S_1 and S_0 states were refined using the CIOpt program developed by the Martinez group.[33] Branching space calculations providing the energy gradient difference vector (GDV) and derivative coupling vector (DCV) at the CIs were performed using the MOLPRO 2010.1 package.[34]

The energies with dynamic correlation were calculated at the multistate CASPT2 level with an imaginary level shift of 0.1 hartree at the CASSCF optimized geometries (MS-CASPT2//CASSCF). All CASPT2 calculations were performed using the MOLCAS 7.6 programs.[35]

3. RESULTS AND DISCUSSION

3.1. Optimized Structures and Energies of Minima on S_0 and S_1 States. All SA3-CASSCF(12e/10o)/6-31G(d)

Table 1. Key Geometry Parameters (bond distance in angstroms and dihedral angles in deg) and the CASSCF and CASPT2//CASSCF Relative Energies (kcal/mol) for the S_0 and S_1 Minima of SP and MC Forms and S_1/S_0 Minimum Energy Conical Intersections (MECIs)

	geometry parameters					relative energy					
	CASSCF					CASSCF			MS-CASPT2		
structure	CO	α	β	γ	τ	S_0	S_1	S_2	S_0	S_1	S_2
					S_0-Min						
S_0-SP*c*	1.422	101.6	1.6	9.5	183.6	0.1	129.7	131.8	0.0	111.6	113.2
S_0-SP*t*	1.424	142.6	−1.9	−10.2	177.8	0.0	129.0	131.9	0.3	111.1	113.9
S_0-CCC	3.146	4.6	−42.1	−8.0	168.4	25.5	106.3	124.9	25.1	96.3	104.3
S_0-TCC	3.130	174.8	58.3	4.4	188.4	26.1	103.3	137.4	34.1	104.2	126.0
S_0-CCT	5.196	2.5	−56.1	177.8	173.8	21.5	98.7	129.2	29.4	99.5	120.7
S_0-TCT	5.170	177.4	64.2	−177.3	185.6	22.8	100.3	131.7	31.2	101.4	123.6
S_0-CTC	4.231	0.0	180.0	0.0	180.0	19.8	97.5	125.2	26.5	97.7	110.6
S_0-TTC	4.231	180.0	180.0	0.0	180.0	19.2	95.8	121.4	23.5	93.7	106.6
S_0-CTT	5.052	0.0	180.0	180.0	180.0	18.7	96.2	121.3	24.7	95.9	109.7
S_0-TTT	5.028	180.0	180.0	180.0	180.0	18.5	95.9	121.2	24.0	95.2	108.9
					S_1-Min						
S_1-SP	1.453	140.2	−4.5	−6.9	176.5	12.3	122.5	155.3	4.9	96.2	131.5
S_1-TCC	3.074	178.7	71.8	5.2	183.3	50.2	78.9	128.0	51.7	87.0	125.0
					S_1/S_0 MECI						
$CI_{S1/S0}$(CCC)	2.638	61.7	10.2	37.4	179.6	66.5	67.8	102.6	45.2	68.8	99.4
$CI_{S1/S0}$(TCC)	2.510	146.2	−7.4	−31.1	181.3	72.9	73.2	117.2	42.4	69.1	105.8
$CI_{S1/S0}$(CN)	1.375 (2.200)[a]	89.4	2.6	3.4	185.3	70.8	69.2	142.2	72.2	60.6	143.6
$CI_{S1/S0}$(CXC)	2.471	4.3	76.8	−0.8	182.0	86.9	87.1	159.1	87.0	90.1	159.6

[a]CN distance.

optimized geometries on the S_0 and S_1 states are summarized in Table 1. Figure 1 shows the two ground-state SP conformers.

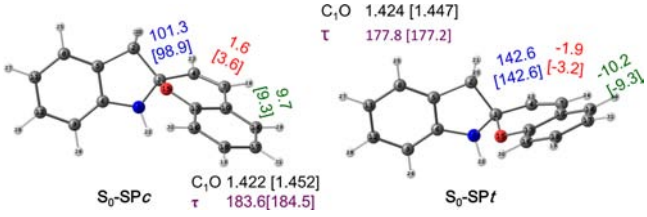

Figure 1. Geometries (bond distance in angstroms and dihedral angles in degrees with α in blue, β in red, and γ in green) of two S_0-SP conformers optimized at the CASSCF(12e/10o)/6-31G(d) level of theory [CAM-B3LYP/6-31G(d) optimized geometry parameters are shown in square parentheses].

The S_0-SP*c* conformer with a bent-down (α = 101.3°) chromene subunit has been previously reported by Sheng et al. at the B3LYP/6-31G(d) level (α = 100.7°),[36] and a similar structure has been obtained at the CASSCF level by Sanchez-Lozano et al. in the *m*SP model (α = 102.6°).[26] The other conformer (S_0-SP*t*) with also the same energy but larger α dihedral angle (α = 142.6°), to our knowledge, has not been reported before. The SP*c* and SP*t* conformers in Figure 1 can be mutually converted by the geometry adjustment of the six-membered (2H-pyran) ring. The cooperation of indoline and benzene moieties distorts the 2*H*-pyran from planar to a bent-down (S_0-SP*c*) and a bent-up (S_0-SP*t*) conformer, respectively. A planar structure (same as that in unsubstituted 2*H*-pyran) acts as the transition state between them. As seen in Figure 1, the adjustments mainly follow the α torsional mode around the C_1-C_2 single bond (as well as torsional modes around C−O bonds), while the double bonds (β and γ) play no roles in the relaxation. Therefore, the interconversion is rather easy. The transition state optimized at the CAM-B3LYP/6-31G(d) level has a barrier height of less than 1.0 kcal/mol, confirming that the above-mentioned conversion takes place easily at room temperature. Considering the small difference in energy and geometry, S_0-SP*c* and S_0-SP*t* should have similar abundance by thermal distribution.

It is also mentioned here that dynamic correction in some cases changes the shape of the PES and therefore the shallow minima at the CASSCF level may disappear at the CASPT2 level. In such a case, geometry optimization at the CASPT2 level is strongly desired (for instance, as we previously did in the photolysis of nitrate radical and ketene molecule[37]). Unfortunately, for such a molecular system with tens of atoms, CASPT2 geometry optimization is still prohibited due to expensive computational costs.

This finding, i.e., both a SP*c* and a SP*t* conformer located in the ground-state PES, is interesting because the large thermal torsional freedom (in the gas phase) will not be suddenly frozen and these "active" torsional modes play roles in the photoinitiated dissociation. Actually, the rotation of a chromene moiety around the torsional coordinate (especially the α bond) on excited-state PES is a product-determining mode for the formation of CCC (cis−cis−cis) and TCC intermediate. In this study, S_0-SP*c* and S_0-SP*t* are used as starting geometry toward CCC and TCC paths, respectively.

The eight isomers of MC, recognized by the conformation referenced to the α, β, and γ bonds, respectively, are also obtained at the SA3-CASSCF(12e,10o)/6-31G(d) level and summarized in Table 1. Only the TCC and CCC forms are directly produced from the light-induced ring-opening steps from SP and will be discussed in detail, while other MC isomers

dx.doi.org/10.1021/ja402868b | J. Am. Chem. Soc. 2013, 135, 10693−10702

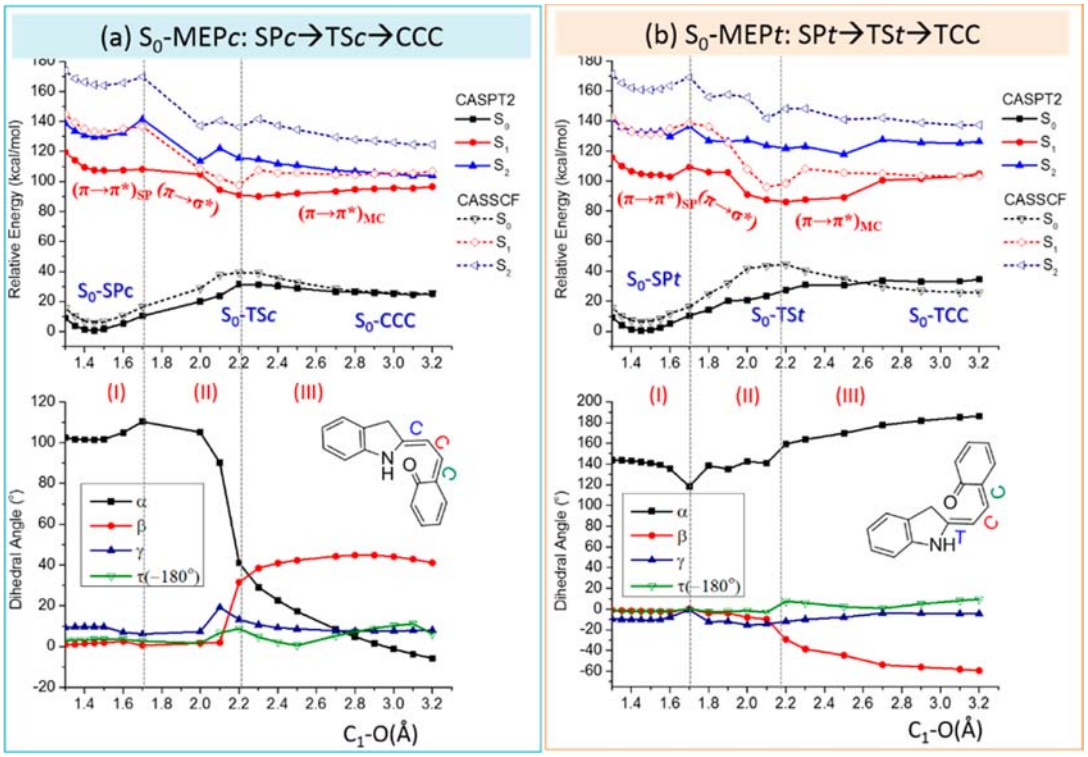

Figure 2. The S_0 minimum energy paths: (a) S_0-MEP*c*: SP*c*→TS*c*→CCC and (b) S_0-MEP*t*: SP*t*→TS*t*→TCC ring-opening reaction, determined by the relaxed S_0 energy scan as a function of the C_1−O distance. Top: The CASPT2//CASSCF (solid line and symbols) and CASSCF (dash line with hollow symbols) energies of S_0, S_1, and S_2 states along the S_0 MEPs. Bottom: Variation of important dihedral angles for S_0 with respect to the C_1−O stretch. Three reaction stages are divided according to the nature of the S_1 state: (I) initial excitation stage, i.e., excitation from S_0-SP to the $(\pi\rightarrow\pi^*)_{SP}$ state, (II) C−O bond-cleavage stage on the $(\pi\rightarrow\sigma^*)$ state, and (III) MC intermediate formation on the $(\pi\rightarrow\pi^*)_{MC}$ state.

and related MC isomerization processes are beyond the scope of this paper.

In the following section (3.2), we will first briefly present the ground-state ring-opening reaction from SP to CCC and TTT. To facilitate the discussion, hereafter they are abbreviated as S_0-MEPc and S_0-MEPt, respectively. In section 3.3 we present the S_1-MEP's starting from the FC-SP(S_1) structure to different branches, i.e., the photochromic C_1−O bond cleavage toward possible CCC(S_1) and TCC(S_1) intermediate (shortened as S_1-MEPc and S_1-MEPt), and an IC path through $MECI_{CN}$ following C_1−N stretching coordinate. In section 3.4, we will discuss the C_1−O bond cleavage on the $(\pi\rightarrow\sigma^*)$ surface, with a detailed discussion on the S_1/S_0 nonadiabatic decay along the $(\pi\rightarrow\sigma^*)$ path as well as the role of the hydrogen-out-of-plane (HOOP) mode.[38,39] The proposed mechanism for the primary ring-opening step of the SP photochromic reaction in this paper is expected to provide clues for understanding the efficient internal conversion process and rationalizing the spectroscopy results of SP−MC isomerization.

3.2. Ground-State Ring-Opening of SP: S_0-MEP*c* and S_0-MEP*t*. The ground-state isomerization (thermal isomerization) between SP and MC has been the topic of many theoretical studies, including the comprehensive investigation by Sheng et al. at a DFT level.[36] Therefore, it is not the main objective of the current study. Tracking the geometrical and electronic structure evolution along the relatively well-established S_0-MEP's can help us to understand the nature of the unexplored excited state; therefore, the S_0-MEP will be presented briefly in this section.

Relaxed energy scans along the C−O distances have been performed at the SA3-CASSCF(12e/10o)/6-31G(d) level and the obtained ground-state C−O cleavage MEP's are shown in Figure 2 for the pathway through S_0-TS*c* (a, top) and S_0-TS*t* (b, top). In the previous DFT calculations by Sheng et al., the path to TCC has been missed due to their failure to obtain the S_0-TS*t* transition state.[36] The barrier heights for the forward reactions SP to MC through TS*c* and TS*t* are nearly identical, 30.4 and 30.9 kcal/mol, respectively, at the MS-CASPT2//CASSCF level, in line with the CAM-B3LYP results (TS*t*, 27.2; TS*c*, 26.8 kcal/mol). If no further reactions are considered, the possibly formed CCC and TCC intermediates will easily switch back to SP either via very low barriers (6.1 kcal/mol for TS*c*) or barrierlessly (−3.7 kcal/mol for TS*t* at the MS-CASPT2//CASSCF level). The major differences between S_0-MEP*c* and S_0-MEP*t* along the C−O elongation coordinate, as seen from the bottom drawings of Figure 2, are remarkable changes to different directions in α (from ∼100° toward 0° for S_0-MEP*c* and from ∼140° toward 180° for S_0-MEP*t*) and also in β (∼0° toward 40° for S_0-MEP*c* and 0° toward −60° for S_0-MEP*t*).

Along the S_0-MEP paths, the nature of excitation from the S_0 to S_1 state changes as C_1−O stretches. The CASSCF S_1 energy profile (shown as a red, dashed line and hollow symbols, along the S_0 MEP geometries) can be divided into three regions (separated by a vertical, black, dashed line) by its nature. In the first region with short C−O distance ($1.4 < C_1\text{−}O < 1.7$ Å), classified as reaction stage I, where the C_1−O bond has been stretched but is still not fully ruptured with relatively little changes in dihedral angles (bottom of Figure 2), the S_1 state still corresponds to the $(\pi\rightarrow\pi^*)$ excitation of the SP molecule. The second stage (II in Figure 2) is between ∼1.7 and ∼2.2 Å in the C−O distance. The characteristic downhill slope of the S_1 energy curve resulting from the $(\pi\rightarrow\sigma_{CO}^*)$ excitation leads

dx.doi.org/10.1021/ja402868b | J. Am. Chem. Soc. 2013, 135, 10693−10702

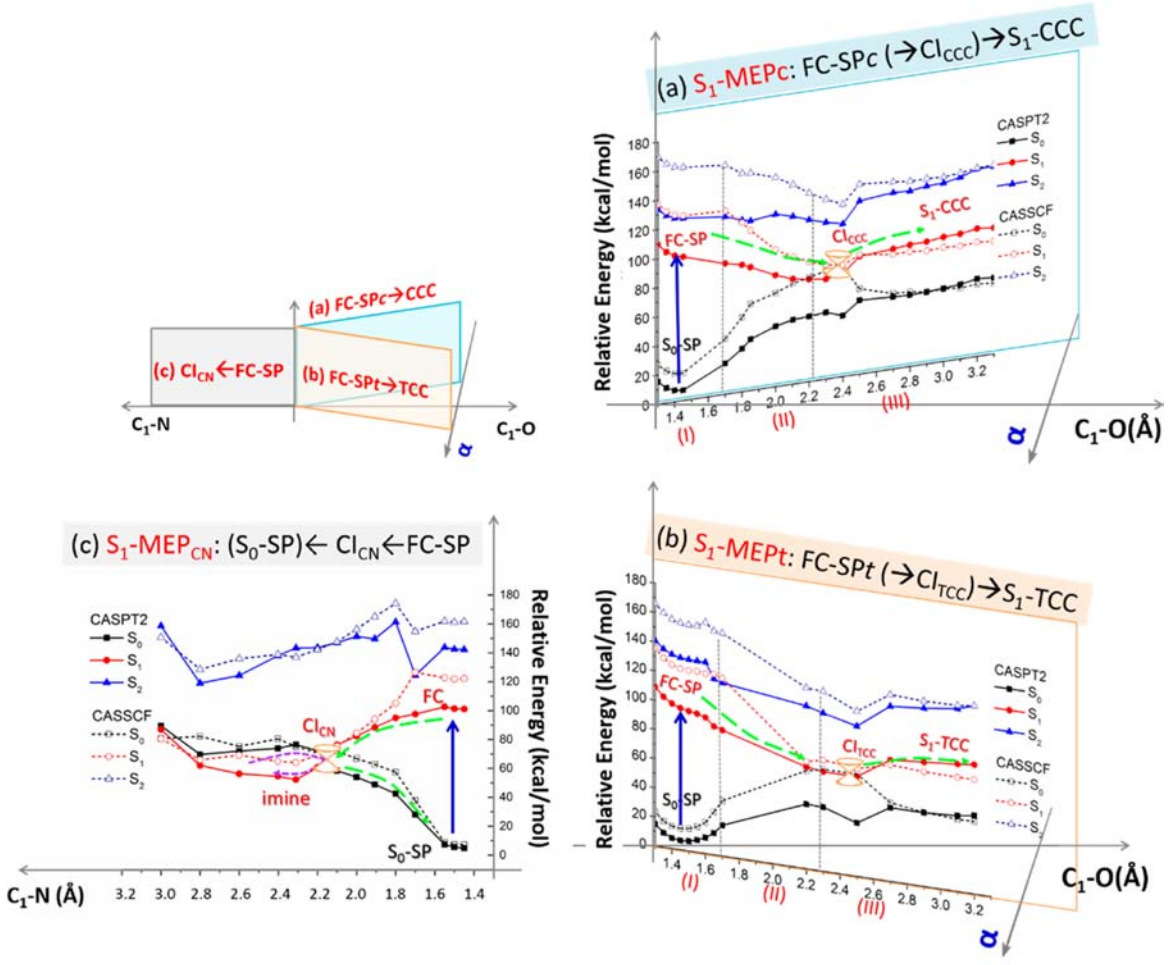

Figure 3. The MS-CASPT2//CASSCF (solid curve and symbols) and CASSCF (dash line with hollow symbols) S_1-MEP's for ring-opening reaction of (a) S_1-MEPc, FC-SP*c* → CCC(S_1) path; (b) S_1-MEPt, FC-SP_t →TCC(S_1) path; and (c) S_1-MEP_{CN}, FC-SP → CI_{CN} path. On each figure, the green, broken arrows indicate the favorable reaction pathway; the funnel icons indicate the crossing points between S_1 and S_0 states (based on optimized structure on S_1-MEPs. Note: They are topologically equal to (but not the same as) optimized $CI_{S1/S0}$ shown in Table 1). All energies are related to that of the global minimum on the S_0 state (S_0-SP).

to an easy C_1-O bond cleavage process. In this stage, the molecule in the S_0 state shows largest geometric changes, as discussed in a previous paragraph. The dihedral angles of the active H ($-C_2$) atom with respect to $C_2-C_1-C_3$ (denoted as τ in Chart 2) are also shown in Figure 2. Along the S_0-MEP, τ shows a very small fluctuation and its value is roughly 0°, indicating a planar C_2 center. In this state, the major torsion is the one around the α bond, therefore corresponding to a one-bond-flipping (OBF) mechanism. This will be discussed in detail later in section 3.4.

After this stage, in stage III, the open-form MC intermediate is formed, which favors an extended conjugated electronic structure; therefore, $(\pi\rightarrow\pi^*)_{MC}$ again becomes the dominant excitation to the S_1 state. The detailed S_1 reaction pathways are discussed in the next section.

In addition to the nature of S_1, it would be of strong interest to understand the character of S_2 along the above-discussed process. The well-separated, highly energetic S_2 state (blue curves in Figure 2) along the reaction coordinate mainly results from $(\pi\rightarrow\pi^*)$ excitation, accompanied by relatively insignificant charge redistribution between the indoline and chromene subunits. Namely, the S_2 state is a weak charge-transfer (CT) state and is inactive in the $C-O$ bond-cleavage process. We expect that the CT excited state may be involved in the consequent process, in which the MC intermediates (CCC or TCC) relax to more stable MC isomers (for instance, TTT and TCC). Due to the absence of the strong electron-withdrawing substituents (for instance, a NO_2 group) at the phenoxide moiety, the CT nature of excited-state unsubstituted MC is substantially weaker than that of their nitro-substituted analogues (for instance, 6-nitro-BIPS).

3.3. Photochromic Ring-Opening of SP: S_1-MEP*c*, S_1-MEP*t*, and S_1-MEP_{CN}. In the S_1 state, at the CASSCF level (Table 1) one conformer that is the $(\pi\rightarrow\pi^*)_{SP}$ state and has an SP*t*-like structure was obtained. The shallow minimum disappears at the CASPT2//CASSCF level and is not likely to be significant.

S_1-MEPc. Figure 3a illustrates the S_1-MEP*c* starting from the FC structure of S_0-SP*c*. Both the CASSCF and MS-CASPT2 energy profiles suggest a smooth, almost barrierless evolution from the initial $(\pi\rightarrow\pi^*)_{SP}$ state to the dissociative $(\pi\rightarrow\sigma^*)$ state. Along the cooperative motion of $C-O$ elongating and α bond torsion (geometry evolution along $C-O$ coordinate will be discussed later in Figure 4), the molecule slides down the downhill slope of the $(\pi\rightarrow\sigma^*)$ surface and meets with an MECI with S_0 surface around the $C-O$ distance of ~2.2 Å. The

dx.doi.org/10.1021/ja402868b | J. Am. Chem. Soc. 2013, 135, 10693−10702

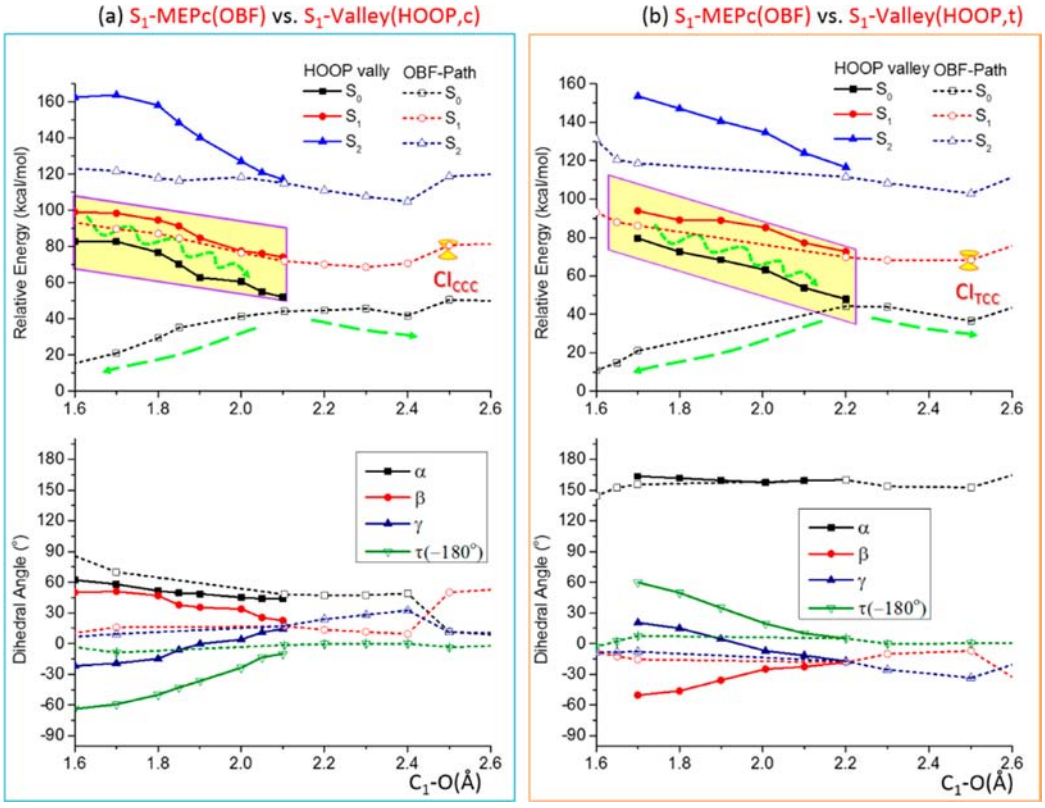

Figure 4. The S_1-MEP's(OBF) paths and S_1-HOOP-valley for (a) SP→CCC and (b) SP→TCC. Top: The CASPT2//CASSCF for HOOP valley (solid curve and symbols) and OBF path (dash line with hollow symbols). Bottom: Geometry variations of important dihedral angles with respect to C_1−O elongation coordinate [for dihedral angle τ, $\tau - 180$ ($0 \leqslant \tau \leqslant 360°$) is plotted]. The ($\pi \rightarrow \sigma^*$) stages are emphasized with a yellow background. Green arrows indicate the possible S_1-to-S_0 radiationless decay and consequent evolution in the S_0 state.

CASSCF-optimized MECI, $CI_{S1/S0}$(CCC), shown in Table 1, can be easily be reached along the S_1-MEP*c*, since the energy of the S_1 state at this point is quite low. Therefore, an efficient funnel through the $CI_{S1/S0}$(CCC) on the S_1-CCC path is expected at the CASSCF level. However, the MS-CASPT2//CASSCF calculations with dynamic correlation shows that the S_1 state is very much higher (>20 kcal/mol, Table 1) than S_0 at this CASSCF $CI_{S1/S0}$(CCC) geometry. The S_1 state remains higher than S_0 in other parts of the S_1-MEP*c*. Therefore at the MS-CASPT2 level, $CI_{S1/S0}$ will be far away from the S_1-MEP*c*, and along the S_1-MEP*c*, the S_1 and S_0 states seem to form an avoided crossing, resulting in a weak nonadiabatic coupling between the two states.

Continuing on S_1-MEP*c*, CASSCF optimization attempts for a CCC(S_1) intermediate all reached the vicinity of S_1/S_0 CIs, such as $CI_{S1/S0}$(CCC) and a nearby $CI_{S0/S1}$(CXC), which lies on the isomerization path of the CCC and CTC forms (which will not be discussed in this paper).

S_1-MEPt. Similar results were found on the S_1-MEP*t* from FC-SP*t* to TCC(S_1), as shown in Figure 3b. The CASSCF S_1/S_0 MECI, $CI_{S1/S0}$(TCC), slightly higher in energy than $CI_{S1/S0}$(CCC), was found along the S_1-MEP*t*. Again, at the MS-CASPT2 level, S_1 remains substantially higher than S_0 along the CASSCF S_1-MEP*t* and an avoided crossing is found. A metastable excited-state intermediate, S_1-TCC, as the product of the current path was obtained at the CASSCF level, although it is energetically higher than the located MECI. It is noticed that in Figure 3a,b the data points (optimized structures) on S_1-MEP at the ($\pi \rightarrow \sigma^*$) region are rather sparse. This is due to the difficulty in obtaining converged geometries at the CASSCF level (The PES at this stage, along the torsional coordinates, is possibly too flat to trap a local minimum). However, we consider that the MEP points connecting stages I and II are sparse but continuous. On one hand, the obtained geometries are located with similar reaction coordinates with those of S_0-MEP, i.e., similar torsion around α, β, and γ bonds with respect to the elongation of C−O distance, suggesting that the S_1-MEP show the same behavior with well-defined S_0-MEP in the ($\pi \rightarrow \sigma^*$) region. As seen in Figure 4 [S_1-MEP's(OBF)], the reaction coordinates in the beginning and end of this region (stage II) show continuous trends. Therefore, the MEP here, although with many missing points, in our opinion, is continuous along the investigated region.

As discussed above, minimum energy paths on S_1 both toward SP CCC and TCC find avoided crossing with a large energy gap with S_0 and suggest that they would not provide efficient internal conversion pathways. Therefore, there must be some other pathways for fast internal conversion found by spectroscopic studies.[18,22] The recent CASSCF study by Sanchez-Lozano and co-workers[26] using a model SP (*m*SP) suggested the C_1−N dissociation route as an efficient internal conversion path.

S_1-MEP$_{CN}$. Therefore, we calculated the S_1-MEP from the FC excited SP molecule (with S_0-SP*c* structure) along the C−N stretching coordinate at the CASSCF(12e/10o)$_{CN}$/6-31G(d) level with the σ/σ^* pair of orbitals for C−N, instead of C−O, included in the active space. The results are shown in Figure 3c, where the C−N stretch is represented by the horizontal axis increasing from right to left. The excited SP molecule on the $(\pi \rightarrow \pi^*)_{SP}$ state can also access the ($\pi \rightarrow \sigma_{CN}^*$) state

dx.doi.org/10.1021/ja402868b | J. Am. Chem. Soc. 2013, 135, 10693−10702

barrierlessly (following the green arrows). The ($\pi\rightarrow\sigma_{CN}$*) and close-shell ground-state PESs intersect near C_1−N = 2.2 Å, after which the ($\pi\rightarrow\sigma_{CN}$*) state became lower in energy than the close-shell one, and an open-shell imine intermediate is formed. The crossing nature in this region is confirmed also in the MS-CASPT2//CASSCF potential curves. The optimized MECI, $CI_{S1/S0}$(CN), is energetically more favorable than the MECIs on the C_1−O dissociation paths by ∼8 kcal/mol (MS-CASPT2//CASSCF; see Table 1). In addition, it is noted that the open-shell metastable imine intermediate, lying in a shallow valley (between C−N coordinate 2.2 to 3.0 Å), can isomerize back to the ground-state SP form. Therefore, both a direct decay process through the CI funnel [FC-SP → $CI_{S1/S0}$(CN) → S_0-SP, green arrows] and a slower process involving an imine intermediate (purple arrows) are expected to contribute to the high IC quantum yields of SP.

3.4. The C−O Bond Cleavage on the ($\pi\rightarrow\sigma$*) State. From the comparative study on the three competing reaction paths discussed in section 3.3, the fast *internal conversion* of SP can be rationalized by the presence of an efficient C_1−N funnel. However, the pathway of a *photochromic C−O ring-opening process* has not been found and remains puzzling. Actually, the optimized MECIs along the S_1-MEP*c* and S_1-MEP*t* paths, $CI_{S1/S0}$(CCC) and $CI_{S1/S0}$(TCC), indicated by their rather long C_1−O distances (2.638 and 2.510 Å, respectively, see Table 1), are located in the MC geometry relaxation stage (stage III, Figure 3a,b) rather than the ending region of the ($\pi\rightarrow\sigma$*) state (on the right-margin of stage II). They are very late compared to the equivalent MECI, $CI_{S1/S0}$(CN), on the S_1 C_1−N dissociation path. Therefore, both $CI_{S1/S0}$(CCC) and $CI_{S1/S0}$(TCC) for the C_1−O dissociation step are "inactive" CIs that could neither act as an efficient internal conversion funnel nor prompt the reaction toward MC side.

Now we focus on the repulsive ($\pi\rightarrow\sigma$*) state, which has been absent in previously published CASSCF calculations because the model compound is too simplified[25] or necessary C_1−O σ/σ* orbitals are missing in the active space.[26] As suggested by previous spectroscopic and theoretical investigations,[19,40] the repulsive ($\pi\rightarrow\sigma$*) state may not only promote the rapid C−O dissociation, but also be able to trigger ultrafast nonradiative decay such as an internal conversion process. That is, the ($\pi\rightarrow\sigma$*) PES intersects not only with the bound PES of the ($\pi\rightarrow\pi$*) excited states but also with that of the electronic ground state.[40] However, as discussed in a preceding section, the computed MS-CASPT2//CASSCF S_1 ($\pi\rightarrow\sigma$*) MEP's, as seen in Figure 3a,b, are well-separated from the close-shell ground-state PES and do not give rise to any region of strong coupling between S_1 and S_0 states. It was previously suggested (by an experimental investigation combined with theoretical analysis, on a different spiropyran) that efficient $S_1\rightarrow S_0$ internal conversion is related to large conformational changes upon optical excitation and can occur with large energy gaps.[41] However, it is not the case in HSP, since the conformational changes from S_0-SP to S_1-SP (listed in Table 1) are rather small. Does there exist an alternative path, along which the ($\pi\rightarrow\sigma$*) and ground state PESs intersect or avoid crossing with each other?

HOOP Mode and S_1-HOOP-Valley. Actually, the somewhat "discontinuous" potential curves in the ($\pi\rightarrow\sigma$*) region II shown in Figure 3a,b already provide some hints to the problem. Remember that the geometries along the S_0-MEP always give a planar C_2 center (see Chart 2) and follow an OBF mechanism around the α bond. However, it is not the case in the ($\pi\rightarrow\sigma$*) state. Constrained geometry optimizations at fixed C_1−O distances did not converge to such α-OBF structures; instead, they drift away to geometries with a more pyramidalized C_2 center. That is, the optimized geometries show significant hydrogen (on C_2 atom) out-of-plane torsion. In Figure 4a,b overlaying the S_1-MEP*c* and S_1-MEP*t* discussed in the previous section [denoted as S_1-MEP*c*(OBF) and S_1-MEP*t*(OBF), dashed line with hollow symbols], we show the alternative low-energy valley denoted as S_1-Valley(HOOP,c) and S_1-Valley(HOOP,t), emphasized in purple boxes and shown in solid line and symbols for S_1 CCC and TCC pathways, respectively, at the MS-CASPT2//CASSCF level (CASSCF-MEP's are shown in Supporting Information, Figure S2). Compared with the optimized structures along the S_1-MEP(OBF) paths, the geometries on the HOOP valleys are distinctively different. The most significant one is that the τ dihedral angles (Chart 2) are far from the ideal value (∼180°), suggesting that the H−(C_2) bond bends out of the C2−C1−C3 plane. The coexistence of the OBF path and the HOOP valley is one of the most interesting features of the investigated system.

S_1 Energy and S_1−S_0 Gap along the HOOP Valley. As seen from the 1D-energy profiles of Figure 4a (or 4b), at short C_1−O distance (C_1−O < ∼1.8 Å) the HOOP valley is slightly higher in energy than the OBF path. Meanwhile, from the bottom figures it is seen the dihedral angles of optimized structures on the HOOP valley are far from those on the OBF path. Therefore, the initially excited SP molecules are only populated into the OBF path. With the elongation of the C_1−O bond, the HOOP valley approaches the OBF path (as indicated by dihedral angles) and their energies become similar; thus, the molecule in the OBF path has more chances to access the HOOP valley. More interestingly, it is found that the S_0 PEC (solid line in black) under the ($\pi\rightarrow\sigma$*) HOOP valley (solid line in red) shows a downhill slope that is nearly in parallel with the S_1 curve in the whole ($\pi\rightarrow\sigma$*) region. The downhill S_0-PECs (HOOP) and uphill ground-state curve finally connect to each other near the ground state TSs, i.e., the C_1−O distance around 2.0−2.2 Å. The energy gaps are moderate (less than 20 kcal/mol at the MS-CASPT2//CASSCF level and are close to zero at the CASSCF level, as seen in Figure S2 of the Supporting Information). Although the nonadiabatic coupling between S_1 and S_0 is not as strong as that in CI, the long coupling time should make S_1-to-S_0 hopping take place. Therefore, we suggest that the S_1/S_0 interacting region along the ($\pi\rightarrow\sigma$*) repulsive path to be another effective nonadiabatic decay path to the ground state (illustrated in Figure 4 as green arrows). After that, the molecule can either switch back to SP (IC) or continue its way toward the product photoisomerization product.

Structural Origin of the HOOP Valley. The findings here are not common in conventional mechanistic calculation, but similar phenomena, i.e., the large out-of-plane motion of hydrogen, are not new in biological systems. In the cis−trans photoisomerization, for instance, in the primary isomerization of retinal in visual pigment rhodopsin,[38,39,42] the carbon skeletal twisting is always accompanied by fast and active HOOP motion. In the ($\pi\rightarrow\sigma$*) C_1−O dissociation step of the current reaction, once the C−O bond is elongated (to ∼1.7 Å), the constraints applied on the α bond is released. Then the twisting around the α bond becomes a product-determining mode, equivalent to the C−C bond twisting in cis−trans isomerization

dx.doi.org/10.1021/ja402868b | J. Am. Chem. Soc. 2013, 135, 10693−10702

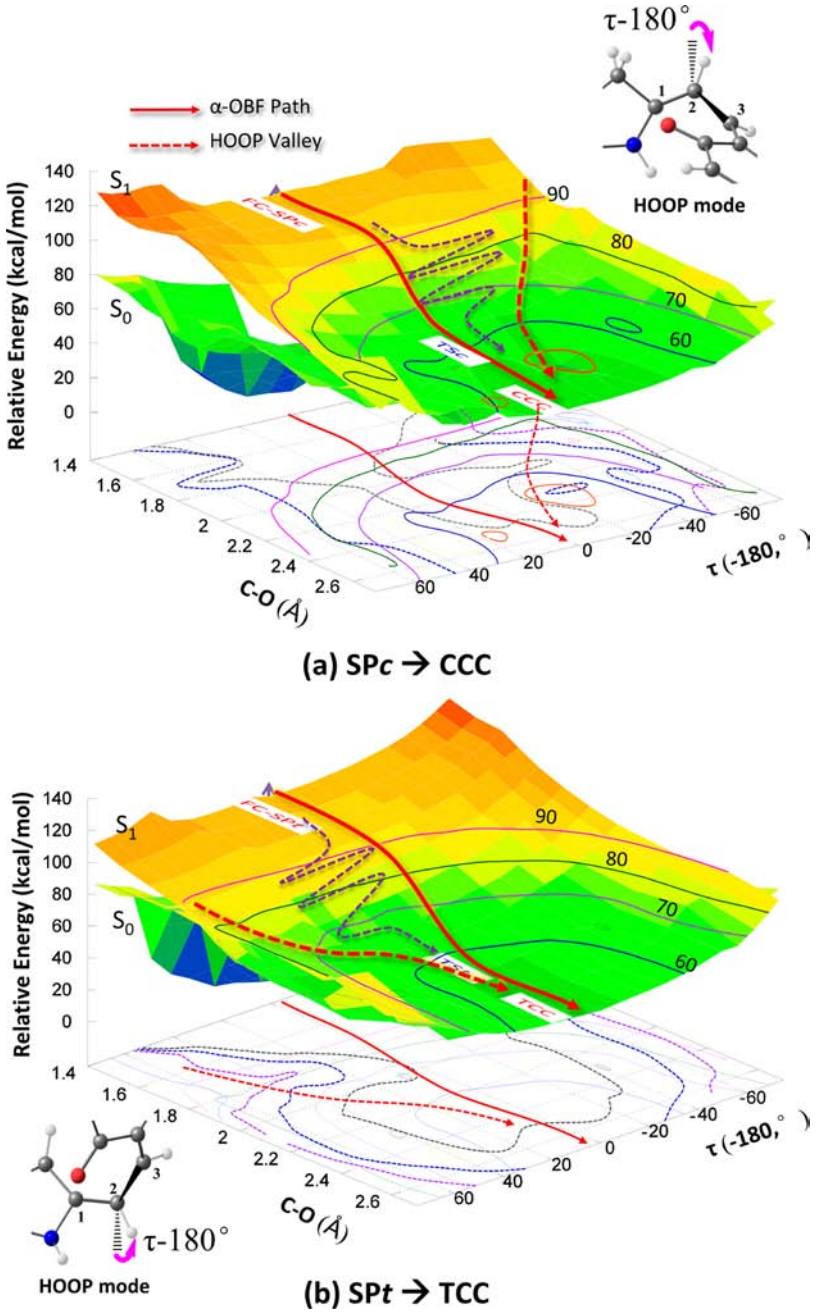

Figure 5. The MS-CASPT2//CASSCF(12e,10o)/6-31G(d) (for N, O) and -/6-31G (for C, H) S_1 and S_0 PESs for (a) FC-SP*c*→CCC and (b) FC-SP*t*→TCC path, respectively. PESs are obtained by 2D constrained geometry optimizations (relaxed scan) along the C_1−O distance and the dihedral angle τ [see Chart 1 for definition; for τ, $\tau - 180$ ($0 \leqslant \tau \leqslant 360°$) is used]. The S_1 contour lines are solid and S_0 are shown as dashed lines with same color scheme. The inset shows the HOOP mode, and the direction of out-of-plane motion is illustrated by pinks arrows.

of the retinal chromosphere, especially in the twist-induced charge-transfer (TICT) stage. In the present system, the H−(C_2) bond is more flexible than the carbon skeletal in the simplified model system (chromene). Therefore, the H−(C_2) bond shows a larger twisting toward the product side, which can be characterized by the dihedral angle τ ($\tau < 180°$ for CCC and $\tau > 180°$ for TCC branch, respectively) shown in Figure 4 (bottom figures). Therefore, the S_1-Valley(HOOP,c) and S_1-Valley(HOOP,t) are competing pathways for the (π,σ*) C_1−O dissociation step with comparable importance with the OBF path.

HOOP Valley Illustrated in 2D PESs. The efficiency of the proposed S_1-HOOP pathways as alternative and efficient IC routes would be best to verify in an on-the-fly molecular dynamic study. This, however, would require very heavy computing and should be a subject of a future study. Here, in order to obtain more detailed information about the PESs for the (π→σ*) C_1−O dissociation step, we carried out a 2D relaxed scan on the S_1 state along the C_1−O distance and the pyramidalization angle τ (defined as H−C_2−C_1−C_3; see Chart 2), using the same active space (12e,10o) but a mixed basis sets [6-31G(d) for N,O and 6-31G for C,H, respectively] at the SA3-CASSCF level. Parts a and b of Figure 5 show the MS-CASPT2//CASSCF PESs for the FC-SP*c*→CCC and FC-SP*t*→TCC processes, respectively. Take the CCC path (Figure 5a), for example. After SP is excited to FC-SP*c*(S_1), it decays

dx.doi.org/10.1021/ja402868b | J. Am. Chem. Soc. 2013, 135, 10693−10702

toward the CCC(S_1) intermediate, along an OBF path around the α bond (solid, red arrow). Also it is noticed that, in the region with the C_1−O distance of 1.7−2.0 Å, both S_1 and S_0 PESs are relatively flat along the τ coordinates. Therefore, the excited SP(S_1) can be promoted by the active HOOP modes (purple arrows) to an alternative, low-energy valley on S_1 (dashed, red arrow). The S_0 surface at the same region shows a downhill slope (rather than uphill, as seen in the close-shell S_0 state along S_0-MEPc in Figure 2a). Despite less accurate results with the smaller basis set, we still see narrow S_1/S_0 gaps along in this region (<∼20 kcal/mol). Therefore, the S_1/S_0 interaction in the ($\pi\rightarrow\sigma^*$) C_1−O bond cleavage process will lead to S_1 to S_0 nonadiabatic decay.

The located HOOP valley, as well as the narrow gap between S_1 and S_0 state, opens a possible radiationless $S_1\rightarrow S_0$ transition channel. The relatively easy-to-access HOOP funnel, in addition to radiationless decay along C−N dissociation, accounts for the high internal conversion yields of SP. The interpretation here is qualitative. Is the role of the HOOP valley overinterpreted or not? We hope a future dynamic simulation or/and ultrafast time-resolved spectroscopic study can make it clear.

4. CONCLUSIONS

In summary, we carried out CASSCF and CASPT2 studies on the reaction mechanism of the photochromic ring-opening process of spiropyran. Possible S_1 reaction paths for C−O and C−N bond cleavages as well as the nonadiabatic transition channel to the ground state were explored. The following conclusions are drawn:

(1) For the primary C−O bond cleavage step of the SP, our CASPT2//CASSCF study does not support a widely accepted conical-intersection mechanism (as proposed in a model study with a simplified benzopyran).[27] The CASSCF-optimized MECIs on the C−O bond-cleavage paths correspond to avoided crossings with a large S_1−S_0 energy gap (>20 kcal/mol) at the CASPT2 level, and thus could not act as efficient internal conversion funnels nor prompt the reaction toward the ground-state MC side. It suggests that, in order to understand the complex mechanism of SP−MC interconversion as well as to interpret the experimental findings, a minimal model with both indoline and chromene moieties is necessary.

(2) Based on the CASPT2//CASSCF PESs, we proposed a new and efficient nonadiabatic decay channel from S_1 to S_0 state. The excited-state molecule distributed on the S_1-MEP(OBF) path can easily access an energy favorable S_1-HOOP-valley following the C−O stretching and H−(C_2) out-of-plane torsion modes. The narrow S_1−S_0 energy gap and long interacting time at the HOOP valley make it an efficient nonadiabatic decay channel. The newly found HOOP funnel, in addition to the decay through a conical intersection on C−N dissociation, account for the high internal conversion yields of SP detected in spectroscopic experiments.

(3) For the C−O dissociation step, the reaction paths leading to both CCC(S_1) and TCC(S_1) intermediates are accessible. The MEPs toward both intermediates are barrierless at the CASPT2//CASSCF level, which are consistent with experimental observation (ultrafast formation of MC form). The S_1-CCC has been failed to be located, while the S_1-TCC may exist as a metastable intermediate. Considering the efficient IC conversion taking place in the ($\pi\rightarrow\sigma^*$) stage, the reaction may have little chance to preceded to the S_1 MC intermediates region; therefore, neither S_1-CCC nor S_1-TCC could be detectable experimentally.

The current study successfully rationalized the ultrafast photochromic ring-opening reaction of SP as well as its efficient internal conversion. The findings here shed light on the complex SP−MC interconversion mechanism and provide foundational information for interpreting experimental findings and designing new spiropyran-based photochromic devices. To explore the details of the HOOP valleys and to elucidate their suggested roles, ultrafast dynamics, for instance, by a time-resolved UV−visible absorption spectroscopic study with isotopically (e.g., deuterium) substituted spiropyran, is high desired.

■ ASSOCIATED CONTENT

Supporting Information

Figures S1−S5 and Cartesian coordinates for the key structures. This material is available free of charge via the Internet at http://pubs.acs.org.

■ AUTHOR INFORMATION

Corresponding Author

morokuma@fukui.kyoto-u.ac.jp

Notes

The authors declare no competing financial interest.

■ ACKNOWLEDGMENTS

This work is in part supported by Japan Science and Technology Agency (JST) with a Core Research for Evolutional Science and Technology (CREST) grant in the Area of High Performance Computing for Multiscale and Multiphysics Phenomena and in part by grants from Japan Society for the Promotion of Science (Grants-in-Aid for Scientific Research <KAKENHI> No. 24245005 at Kyoto University). F.L. is grateful to Dr. Lung Wa Chung and Zhuofeng Ke for helpful discussions. The computational resource at Research Center of Computer Science (RCCS) at the Institute for Molecular Science (IMS) and Kyoto University Supercomputer System is also acknowledged.

■ REFERENCES

(1) Berkovic, G.; Krongauz, V.; Weiss, V. *Chem. Rev.* **2000**, *100*, 1741−1754.

(2) Parthenopoulos, D. A.; Rentzepis, P. M. *Science* **1989**, *245*, 843−845.

(3) Feringa, B. L. B. L.; Van Delden, R. A. R. A. R. a.; Koumura, N.; Geertsema, E. M. E. M. *Chem. Rev.* **2000**, *100*, 1789−1816.

(4) Buback, J.; Kullmann, M.; Langhojer, F.; Nuernberger, P.; Schmidt, R.; Würthner, F.; Brixner, T. *J. Am. Chem. Soc.* **2010**, *132*, 16510−16519.

(5) Raymo, F. M.; Giordani, S. *Proc. Natl. Acad. Sci. U. S. A.* **2002**, *99*, 4941−4944.

(6) Fujimoto, K.; Amano, M.; Horibe, Y.; Inouye, M. *Org. Lett.* **2006**, *8*, 285−287.

(7) Darwish, T. a; Evans, R. a; James, M.; Malic, N.; Triani, G.; Hanley, T. L. *J. Am. Chem. Soc.* **2010**, *132*, 10748−10755.

(8) Zhou, W.; Chen, D.; Li, J.; Xu, J.; Lv, J.; Liu, H.; Li, Y. *Org. Lett.* **2007**, *9*, 3929−3932.

(9) Silvi, S.; Arduini, A.; Pochini, A.; Secchi, A.; Tomasulo, M.; Raymo, F. M.; Baroncini, M.; Credi, A. *J. Am. Chem. Soc.* **2007**, *129*, 13378−13379.

(10) Achilleos, D. S.; Hatton, T. A.; Vamvakaki, M. *J. Am. Chem. Soc.* **2012**, *134*, 5726−5729.

(11) Chen, J.; Zhang, P.; Fang, G.; Yi, P.; Yu, X.; Li, X.; Zeng, F.; Wu, S. *J. Phys. Chem. B* **2011**, *115*, 3354−3362.
(12) Osborne, E. a; Jarrett, B. R.; Tu, C.; Louie, A. Y. *J. Am. Chem. Soc.* **2010**, *132*, 5934−5935.
(13) Kamenjicki Maurer, M.; Lednev, I. K.; Asher, S. a. *Adv. Funct. Mater.* **2005**, *15*, 1401−1406.
(14) Albuquerque, R. Q.; Kühni, J.; Belser, P.; De Cola, L. *ChemPhysChem* **2010**, *11*, 575−578.
(15) Tamai, N.; Miyasaka, H. *Chem. Rev.* **2000**, *100*, 1875−1890.
(16) Lenoble, C.; Becker, R. S. *J. Phys. Chem.* **1986**, *90*, 62−65.
(17) Ernsting, N. P.; Arthen-Engeland, T. *J. Phys. Chem.* **1991**, *95*, 5502−5509.
(18) Rini, M.; Holm, A.-K.; Nibbering, E. T. J.; Fidder, H. *J. Am. Chem. Soc.* **2003**, *125*, 3028−3034.
(19) Poisson, L.; Raffael, K. D.; Soep, B.; Mestdagh, J.-M.; Buntinx, G. *J. Am. Chem. Soc.* **2006**, *128*, 3169−3178.
(20) Kullmann, M.; Ruetzel, S.; Buback, J.; Nuernberger, P.; Brixner, T. *J. Am. Chem. Soc.* **2011**, *133*, 13074−13080.
(21) Hobley, J.; Pfeifer-Fukumura, U.; Bletz, M.; Asahi, T.; Masuhara, H.; Fukumura, H. *J. Phys. Chem. A* **2002**, *106*, 2265−2270.
(22) Kohl-Landgraf, J.; Braun, M.; Ozçoban, C.; Gonçalves, D. P. N.; Heckel, A.; Wachtveitl, J.; Özçoban, C. *J. Am. Chem. Soc.* **2012**, *134*, 14070−14077.
(23) Roos, B. O. In *Advances in Chemical Physics*; Lawley, K. P., Ed.; John Wiley & Sons, Inc.: New York, 1987; Vol. *69*, pp 399−445.
(24) Finley, J.; Roos, O.; Serrano-andres, L. *Chem. Phys. Lett.* **1998**, 299−306.
(25) Celani, P.; Bernardi, F.; Olivucci, M.; Robb, M. A. *J. Am. Chem. Soc.* **1997**, *119*, 10815−10820.
(26) Sanchez-Lozano, M.; Estévez, C. M.; Hermida-Ramón, J.; Hermida-Ramón, J.; Serrano-Andres, L. *J. Phys. Chem. A* **2011**, *115*, 9128−9138.
(27) Yarkony, D. R. *Rev. Mod. Phys.* **1996**, *68*, 985−1013.
(28) Liu, F.; Liu, Y.; De Vico, L.; Lindh, R. *J. Am. Chem. Soc.* **2009**, *131*, 6181−6188.
(29) Liu, F.; Liu, Y.; De Vico, L.; Lindh, R. *Chem. Phys. Lett.* **2009**, *484*, 69−75.
(30) Chung, L. W. L. W.; Hayashi, S.; Lundberg, M.; Nakatsu, T.; Kato, H.; Morokuma, K. *J. Am. Chem. Soc.* **2008**, *130*, 12880−12881.
(31) Ditchfield, R. *J. Chem. Phys.* **1971**, *54*, 724−728.
(32) Liu, F.; Morokuma, K. *J. Am. Chem. Soc.* **2012**, *134*, 4864−4876.
(33) Levine, B. G.; Coe, J. D.; Martínez, T. J. *J. Phys. Chem. B* **2008**, *112*, 405−413.
(34) Werner, H.-J.; Knowles, P. J.; Knizia, G.; Manby, F. R.; Schütz, M. *WIREs Comput. Mol. Sci.* **2012**, *2*, 242−253.
(35) Lindh, R. *J. Comput. Chem.* **2010**, *31*, 224−247.
(36) Sheng, Y.; Leszczynski, J.; Garcia, A. a.; Rosario, R.; Gust, D.; Springer, J. *J. Phys. Chem. B* **2004**, *108*, 16233−16243.
(37) Xiao, H.; Maeda, S.; Morokuma, K. *J. Phys. Chem. Lett.* **2011**, *2*, 934−938; *J. Chem. Theory Comput.* **2012**, *8*, 2600−2605. Xiao, H.; Maeda, S.; Morokuma, K. *J. Phys. Chem. A*, Article ASAP (DOI: 10.1021/jp312719a).
(38) Kukura, P.; McCamant, D. W.; Yoon, S.; Wandschneider, D. B.; Mathies, R. A. *Science* **2005**, *310*, 1006−1009.
(39) Weingart, O.; Altoè, P.; Stenta, M.; Bottoni, A.; Orlandi, G.; Garavelli, M. *Phys. Chem. Chem. Phys.* **2011**, *13*, 3645−3648.
(40) Sobolewski, A. L.; Domcke, W.; Dedonder-Lardeux, C.; Jouvet, C. *Phys. Chem. Chem. Phys.* **2002**, *4*, 1093−1100.
(41) Fidder, H.; Rini, M.; Nibbering, E. T. J. *J. Am. Chem. Soc.* **2004**, *126*, 3789−3794.
(42) Li, X.; Chung, L. W.; Morokuma, K. *J. Chem. Theory Comput.* **2011**, *7*, 2694−2698.